Article

Neuron

Proneurogenic Ligands Defined by Modeling Developing Cortex Growth Factor Communication Networks

Highlights

- Model of cortical neuron-cortical precursor communication from transcriptome data
- Integration of cell-surface proteome of neurons/precursors into communication model
- Cortical neuron-precursor communication model predicts proneurogenic ligands
- IFNγ, Nrtn, and GDNF predicted by the model stimulate embryonic neurogenesis

Authors

Scott A. Yuzwa, Guang Yang, Michael J. Borrett, ..., Peter W. Zandstra, David R. Kaplan, Freda D. Miller

Correspondence

dkaplan@sickkids.ca (D.R.K.), fredam@sickkids.ca (F.D.M.)

In Brief

Yuzwa et al. use transcriptome and cell-surface proteome profiling of developing cortical neural precursors and neurons to model cell-cell communication between these two cell types. Testing the resulting integrated model identifies growth factors that promote genesis of neurons.

Accession Numbers

GSE84482

Yuzwa et al., 2016, Neuron *91*, 988–1004
September 7, 2016
http://dx.doi.org/10.1016/j.neuron.2016.07.037

CellPress

Neuron
Article

Proneurogenic Ligands Defined by Modeling Developing Cortex Growth Factor Communication Networks

Scott A. Yuzwa,[1] Guang Yang,[1] Michael J. Borrett,[1] Geoff Clarke,[2] Gonzalo I. Cancino,[1] Siraj K. Zahr,[1,3] Peter W. Zandstra,[2,4,5,6] David R. Kaplan,[1,3,7,*] and Freda D. Miller[1,3,5,7,8,*]
[1]Program in Neurosciences and Mental Health, Hospital for Sick Children, Toronto, ON M5G 1L7, Canada
[2]Institute of Biomaterials and Biomedical Engineering
[3]Institute of Medical Sciences
[4]The Donnelly Centre
[5]McEwen Centre for Regenerative Medicine
[6]Departments of Chemical Engineering and Applied Chemistry
[7]Department of Molecular Genetics
[8]Department of Physiology
University of Toronto, Toronto, ON M5G 1A8, Canada
*Correspondence: dkaplan@sickkids.ca (D.R.K.), fredam@sickkids.ca (F.D.M.)
http://dx.doi.org/10.1016/j.neuron.2016.07.037

SUMMARY

The neural stem cell decision to self-renew or differentiate is tightly regulated by its microenvironment. Here, we have asked about this microenvironment, focusing on growth factors in the embryonic cortex at a time when it is largely comprised of neural precursor cells (NPCs) and newborn neurons. We show that cortical NPCs secrete factors that promote their maintenance, while cortical neurons secrete factors that promote differentiation. To define factors important for these activities, we used transcriptome profiling to identify ligands produced by NPCs and neurons, cell-surface mass spectrometry to identify receptors on these cells, and computational modeling to integrate these data. The resultant model predicts a complex growth factor environment with multiple autocrine and paracrine interactions. We tested this communication model, focusing on neurogenesis, and identified IFNγ, Neurturin (Nrtn), and glial-derived neurotrophic factor (GDNF) as ligands with unexpected roles in promoting neurogenic differentiation of NPCs in vivo.

INTRODUCTION

The self-renewal versus differentiation of neural precursor cells (NPCs) is determined by the interplay between intrinsic mechanisms and the microenvironment where they reside. This microenvironment is comprised, in part, of growth factors secreted by neighboring cells like other NPCs, glial cells, and neurons that are present in the circulation and cerebrospinal fluid (Gauthier-Fisher and Miller, 2013). Previous work has defined individual ligands that regulate embryonic and adult NPCs, including neurotransmitters (Haydar et al., 2000), circulating growth factors (Villeda et al., 2011), and locally produced growth factors like FGF2 and IL-6 (Gallagher et al., 2013; Raballo et al., 2000). Nonetheless, we still lack an overview of the NPC growth factor microenvironment.

How might we obtain such an overview? We have chosen to do so by combining transcriptomic and proteomic profiling to analyze the embryonic murine cortex during the period of neurogenesis. At this time, cortical radial precursors are maintained in a neuroepithelium, with their apical endfeet forming the interface with the lateral ventricles, and their basal processes extending to the cortical surface. These radial precursors generate neurons that delaminate from the apical epithelium and migrate basally in intimate contact with the radial precursor processes (Noctor et al., 2001). To understand the growth factors that are important during this process, we have focused upon these two cell types, radial precursors and their newborn neuronal progeny, and have used an iterative systems biology strategy. We show that cultured cortical precursors secrete factors that promote their own maintenance, while cortical neurons secrete factors that promote neurogenesis. To identify these secreted factors, we defined the transcriptome and cell-surface proteome of cultured cortical precursors and neurons and used these data to model the growth factor communication within and between these two populations. This model predicts a complex growth factor communication network that provides the basis for multiple potential autocrine and paracrine interactions. We tested this model by focusing on growth factors that might enhance neurogenesis, and in so doing, have identified three factors, IFNγ, Nrtn, and GDNF, that are necessary and sufficient for the neurogenic differentiation of radial precursor cells in vivo.

RESULTS

Factors Secreted by Cultured Cortical Precursors and Their Neuronal Progeny Regulate Self-Renewal versus Differentiation

During neurogenesis, the cortex is largely comprised of radial precursors and newborn neurons. To identify secreted ligands

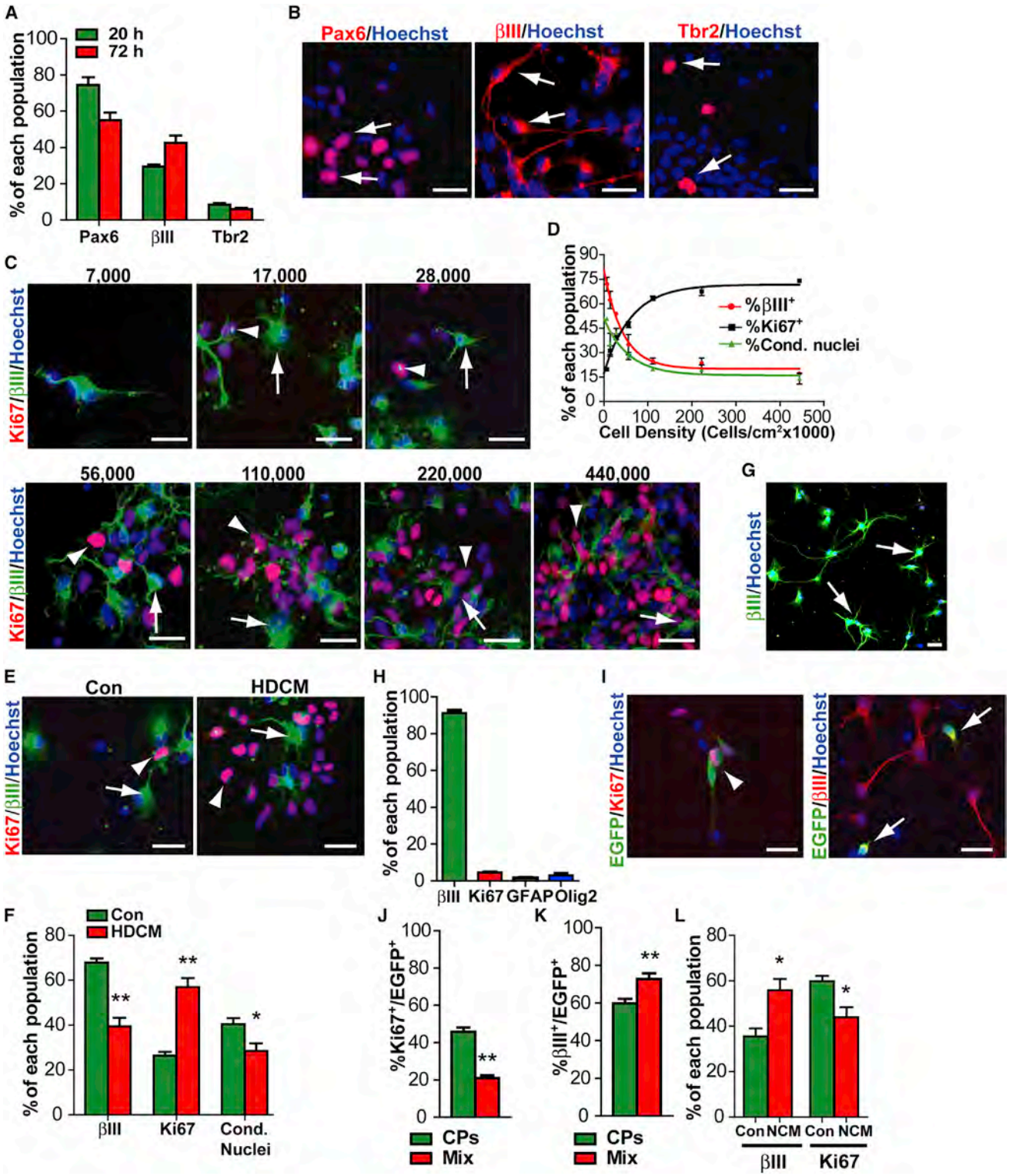

Figure 1. Cortical Precursors and Neurons Secrete Factors to Regulate Cortical Precursor Proliferation and Differentiation

(A and B) E13 precursors were cultured 20 or 72 hr, immunostained for Pax6, Tbr2, or βIII-tubulin (all red in B), and positive cells were quantified (A).

(C and D) E13 precursors were cultured 3 days at 7,000–440,000 cells/cm^2, immunostained for Ki67 (red, arrowheads in C), and/or βIII-tubulin (βIII, green, arrows in C) and quantified (D). Cultures were also quantified for condensed, apoptotic nuclei (D). n = 3 experiments.

(legend continued on next page)

within this microenvironment, we studied embryonic day 13 (E13) cortical cultures that are comprised of proliferating Sox2 and Pax6-positive radial precursors, and a small number of intermediate progenitors, the neurogenic transit-amplifying cells in this system (Gauthier-Fisher et al., 2009; Gallagher et al., 2013). These cultured precursors generate neurons for 4–5 days and then switch to making glia at 6–7 days. Immunostaining confirmed this cellular composition after 20 and 72 hr of culture (Figures 1A and 1B). There were no CD31-positive blood vessel cells, Iba1-positive microglia, GFAP-positive astrocytes, or MBP-positive oligodendrocytes at either time point. Instead, at 20 hr about 75% and 25% of the cells were Pax6-positive radial precursors and βIII-tubulin-positive neurons, respectively. By 72 hr, radial precursors had decreased to about 55%, and neurons had increased. At both time points, 6%–9% of cells were Tbr2-positive intermediate progenitors.

We asked whether these cultures were density dependent by plating E13 precursors for 3 days at 7,000 to 440,000 cells/cm^2. Immunostaining (Figures 1C and 1D) showed that at low cell densities (7,000 to 28,000 cells/cm^2), most precursors differentiated into neurons. As densities increased, the relative proportion of neurons decreased, until at densities $\geq$110,000 cells/cm^2, only 20%–30% of cells were neurons, while 65%–75% were proliferating Ki67-positive precursors. Survival was also increased at higher cell densities (Figure 1D).

To ask whether these density-dependent effects were due to secreted molecules, we collected medium conditioned by high-density cultures (110,000 cells/cm^2) for 3 days. At the time we collected the medium, about 23% of cells were neurons and the rest were precursors. We applied this conditioned medium to E13 precursors cultured at low density (14,000 cells/cm^2). Immunostaining after 3 days (Figures 1E and 1F) showed that in control medium, about 70% and 30% of cells were neurons and proliferating precursors, respectively. In contrast, conditioned medium from high-density cultures reduced this to about 40% neurons and 60% proliferating precursors, proportions similar to those in high-density cultures (Figure 1D). Survival, however, was only modestly reduced by high-density conditioned medium (Figure 1F). Since high-density cultures are mostly precursors, these data indicate that they secrete molecules to enhance their own expansion.

Newborn Cortical Neurons Secrete Factors that Promote Cortical Neurogenesis

We next asked whether newborn cortical neurons also secrete factors that influence cortical precursor biology. To do this, we transfected E13 precursors with plasmids encoding the *piggybac* (PB) transposase and a PB-EGFP reporter that indelibly marks a subset of precursors and all of their progeny (Gallagher et al., 2013). We then isolated and cultured E16 cortical neurons for 4 days. Immunostaining (Figures 1G and 1H) confirmed that almost all cells were βIII-tubulin-positive neurons, with no Iba1-positive microglia, CD31-positive endothelial cells, Pax6-positive radial precursors, CC1- or MBP-positive oligodendrocytes, and only a very few cells expressing the astrocyte marker GFAP, the glial precursor marker Olig2, or Ki67.

We mixed these unlabelled cortical neurons with the transfected, labeled precursors at a ratio of 6:1 precursors to neurons. Immunostaining 1 day later showed that adding unlabelled neurons increased the genesis of EGFP-positive neurons, and concomitantly decreased the EGFP-positive, proliferating Ki67-positive precursors (Figures 1I–1K). To ask whether this pro-neurogenic effect was due to factors secreted by the added neurons, we prepared conditioned medium from the purified cultured neurons and added it, with FGF2 (which is in the basal precursor medium), to freshly plated E13 precursors. Analysis 3 days later showed that, relative to control medium containing FGF2, neuron-conditioned medium increased newborn neurons and decreased proliferating precursors (Figure 1L).

Computational Modeling of Transcriptome Data to Predict Growth Factor Communication within and between Cortical Precursors and Neurons

These data indicate that cortical neurons and precursors secrete factors that promote neurogenesis and proliferation, respectively. To identify the relevant ligands, we used a computational modeling method that makes use of microarray-based transcriptomic data to predict autocrine/paracrine interactions (Qiao et al., 2014). Initially, we performed microarrays on cortical precursors and neurons. For the neurons, we used 5 day cultures, when they were almost a pure neuronal population (see Figures 1G and 1H). For the precursors, we grew E13 cultures at 100,000 cells/cm^2 for 20 hr, at which point they were 75% radial precursors, 5%–10% intermediate progenitors, and 20% newborn neurons (called enriched precursors from hereon) (Figure S1A). We also analyzed a culture containing precursors mixed with purified cortical neurons at a 6:1 ratio. For each population, we isolated total RNA from three independent biological replicates and analyzed it on Affymetrix GeneChip Mouse Gene 2.0 ST Arrays.

This analysis showed that 1,479 genes were at least 2-fold differentially expressed when comparing neurons and enriched precursors ($p < 0.05$ FDR) (Figure 2A; Table S1). Unbiased

(E and F) E13 precursors were cultured 3 days at low density (14,000 cells/cm^2) in control medium (Con), or in medium conditioned by high-density (110,000 cells/cm^2) precursor cultures (HDCM), immunostained for Ki67 (red, arrowheads, E) and βIII-tubulin (green, arrows, E), and quantified (F). Cultures were also quantified for condensed, apoptotic nuclei (Cond. Nuclei, F). *$p < 0.05$, **$p < 0.01$, n = 3 experiments.

(G) Representative image of purified cortical neurons immunostained for βIII-tubulin (arrows, green).

(H) Quantification of cultures as in (G) for the proportion of βIII-tubulin, Ki67, GFAP, or olig2-immunopositive cells. n = 2 cultures.

(I–K) E13 precursors transfected with the *piggybac* EGFP reporter were cultured alone (CPs) or with neurons at a 6:1 ratio (Mix) for 1 day, immunostained for EGFP (green, I) and Ki67 (red, left panel, I) or βIII-tubulin (red, right panel, I), and quantified (J and K). Double-labeled cells in (I) are indicated by arrows or arrowheads. **$p < 0.01$, n = 3 experiments.

(L) E13 precursors were cultured in control medium (Con) or neuron-conditioned medium (NCM) for 3 days, immunostained, and Ki67-positive precursors and βIII-tubulin-positive neurons (βIII) were quantified. *$p < 0.05$, n = 4 experiments. Cultures in (B), (C), and (G) were counterstained with Hoechst 33258 (blue). Scale bars represent 50 μm in (G) and 25 μm in all other panels. Error bars represent SEM.

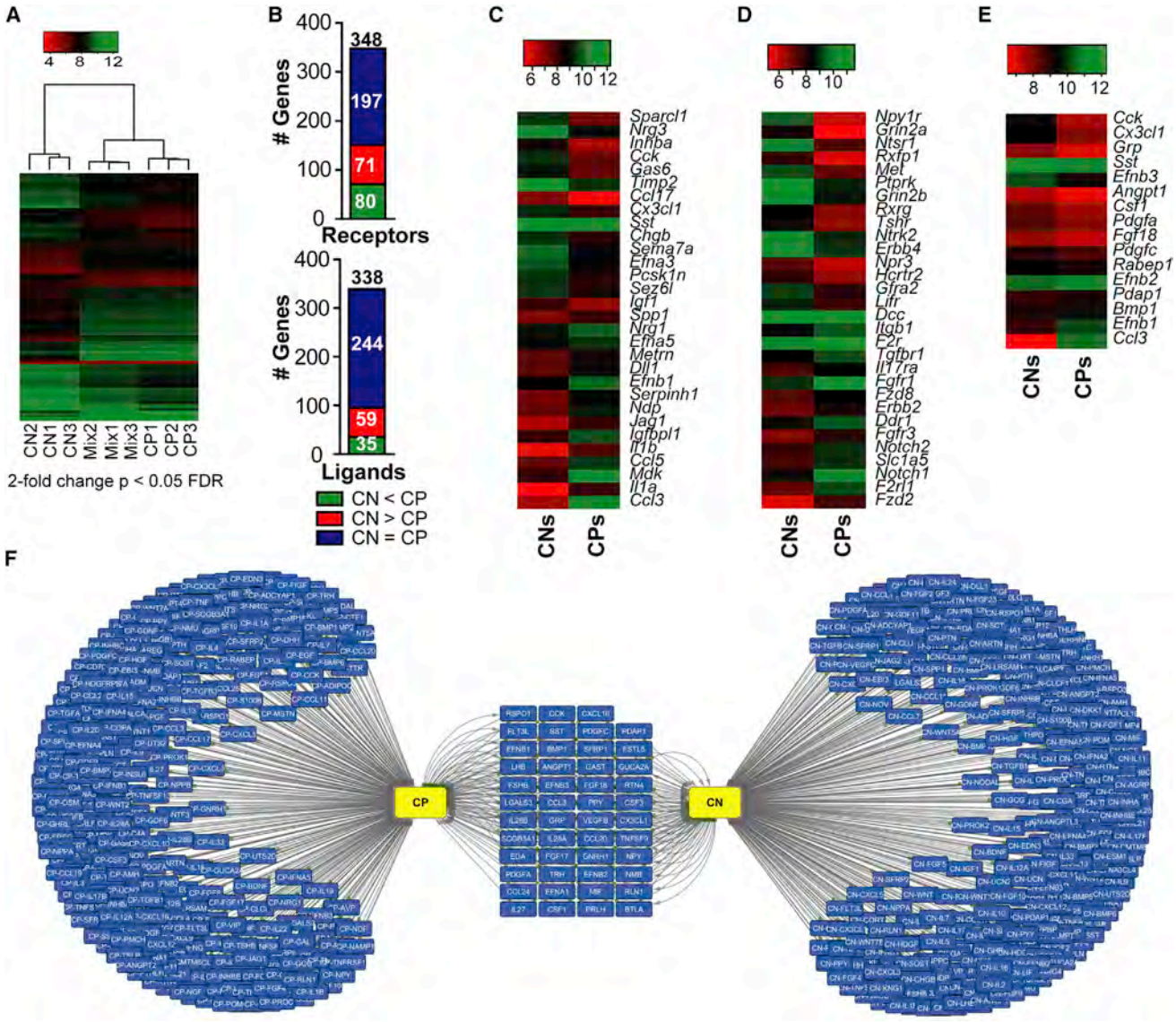

Figure 2. Modeling Embryonic Cortical Precursor/Cortical Neuron Growth Factor Interactions Using Transcriptome Data

Total RNA was isolated from three replicates each of enriched cortical precursors (CPs), cortical neurons (CNs), and a 6:1 ratio of precursors to neurons (Mix), and analyzed on Affymetrix GeneChip Mouse Gene 2.0 ST Arrays.

(A) Heatmap and hierarchical clustering of differentially expressed genes (>2-fold, $p < 0.05$ FDR).

(B) Number of receptor (top) and ligand (bottom) genes expressed in CNs and CPs, classified into those expressed at similar levels in CNs and CPs (blue), and those that were significantly higher in CNs (red) or CPs (green) ($p < 0.05$ FDR).

(C and D) Heatmaps of the average $\log_2$-normalized expression data for the top 15 most highly enriched ligand (C) and receptor (D) genes in CNs (top 15 rows) and CPs (bottom 15 rows).

(E) Heatmap of average $\log_2$-normalized expression data for 16 differentially expressed ($p < 0.05$ FDR) ligand genes predicted to act in a paracrine fashion in the model shown in (F).

(F) Transcriptome-based network model of cortical growth factor communication. Nodes in blue to the left of the yellow CP node are predicted CP autocrine ligands, and to the right of the yellow CN node are predicted CN autocrine ligands. Blue nodes between the yellow CP and CN nodes are predicted paracrine ligands. Any ligand denoted as autocrine for both CPs and CNs could also function in a paracrine fashion. Arrows indicate direction of communication. Also see Figure S1.

hierarchical clustering using the complete-linkage method of an Euclidean distance matrix of $\log_2$ normalized expression data showed that the neuron and enriched precursor replicates each clustered closely and that the mixed population clustered closest to the enriched precursors, likely because the mixed cultures contained more precursors than neurons (20%–25% newborn neurons in the enriched precursors plus 16% added neurons) (Figure 2A). Gene ontology (GO) analysis showed

that, as predicted, differentially expressed genes in neurons versus precursors were highly enriched for processes such as cell cycle, neurogenesis, generation of neurons, and neuron differentiation (Figure S1B). Thus, this approach readily distinguished neurons from enriched precursors.

We next defined the growth factor and receptor mRNAs in these datasets using a curated database of secreted ligands and their cognate receptors (Qiao et al., 2014) (Table S2). Cortical neurons and enriched precursors expressed 338 ligand mRNAs (Table S3), of which 244 were expressed at similar levels in both populations. However, 59 and 35 ligand genes were expressed more highly in neurons and precursors, respectively (Figure 2B; Table S4), with expression differences from 2- to 17-fold (Figure 2C). The most highly enriched neuronal ligands included SPARCL1 (hevin), inhibin βA (as a homodimer, called activin A), growth arrest-specific 6 (Gas6), CCL17 (TARC), and neuregulin 3. The most highly enriched precursor ligands included interleukin 1α, interleukin 1β, midkine (mdk), the Notch ligand Jagged, and the Frizzled 4 ligand Norrin (ndp).

Neurons and precursors also expressed 348 receptor mRNAs (Table S3), with 197 expressed at similar levels. 71 and 80 receptor mRNAs were enriched in neurons and precursors, respectively (Figure 2B; Table S4), with expression differences of 2- to 11-fold (Figure 2D). Receptor mRNAs most highly enriched in neurons included neuropeptide receptors for NPY, neurotensin, and hypocretin and neurotransmitter receptors such as the ionotropic glutamate receptors 2a and 2b. The most highly enriched precursor receptors included Notch 1 and 2, Frizzled 2, and FGF receptors 1 and 3.

We used these transcriptome data to assemble a cortical precursor/cortical neuron communication model (see flow chart in Figure S1C). Initially, we used a perturbation statistical model (PERT) (Qiao et al., 2012) that analyzes gene expression measurements of individual cells alone and when mixed together to calculate how their profiles might change in a heterogeneous environment such as the embryonic cortex. For example, some cytokines upregulate expression of their receptors, so in a mixed population where one population expresses the cytokine and the other the receptor, paracrine cytokine exposure would increase receptor mRNA in the second population. A comparison with the purified populations allows the mixed profile to be deconvolved into its constituent parts and allows the expression profiles of each individual gene to be corrected for the more biologically relevant mixed population conditions.

We used the corrected neuron and enriched precursor reference gene expression profiles together with the curated ligand and receptor database and our previously published methodology for assembling cell interaction networks (Qiao et al., 2014; see the flow chart in Figure S1C) to construct an autocrine/paracrine communication network for the cortical precursor/neuron interactions (Figure 2F; Table S5). In the resultant model, each node is a secreted ligand and each line is a direction of communication from precursor to precursor, neuron to neuron, precursor to neuron, or neuron to precursor. Ligands predicted to be autocrine (acting within the same population of cells) for cortical precursors and cortical neurons are denoted CP and CN, respectively. Ligands denoted as autocrine for both populations (and there are many) could also potentially function in a paracrine fashion. Ligands that are predicted specifically as paracrine (from one cell type to another) are shown as nodes located between the neurons and precursors.

This model supports a number of conclusions. First, it predicts a large number of potential ligand-receptor interactions between the two populations (Figure 2F; Table S5), many of which are known to be important for cortical precursors, including FGF2, EGF, Wnt ligands, neurotrophins, PDGFs, ligands of the gp130 family, BMPs, and Notch (Gauthier-Fisher and Miller, 2013). However, this model also predicts many potential ligand-receptor interactions not previously considered within a neural precursor context such as those involving Gastrin Releasing Peptide (GRP) and CCL3 (macrophage inflammatory protein-1α). Second, these data showed that most ligand and receptor mRNAs are expressed at statistically similar levels in neurons and enriched precursors (Figures 2B and 2F; Table S5). Third, because of the large overlap in precursor and neuron ligands and receptors, the model predicts that many interactions would be both autocrine and paracrine, with only 51 limited to a directional paracrine signal. Of these, 16 involved differentially expressed ligands with 11 enriched in neurons, including cholecystokinin (CCK), fractalkine (CX3CL1), and GRP, and five in precursors, including CCL3, Ephrin-B1, and bone-morphogenetic protein 1 (BMP1) (Figure 2E).

Finally, we asked whether any of the receptors and ligands in this model were highly co-expressed, as might be predicted by their function in a cell-cell communication network, using weighted correlation network analysis (WGCNA). WGCNA on the nine ligand/receptor datasets (three each from precursors, neurons, and the mixed cells) identified clusters of coexpressed receptors and ligands (Figure S1D; Table S5). By comparison, WGCNA on a similar number of randomly selected genes in the parent microarray datasets did not generate these coexpression modules (Figure S1E). These modules were relevant for both precursors and neurons, as shown by overlaying them on the communication network (Figure S1F), and included ligand/receptor groups known to be important in the embryonic cortex, including, in the cluster color-coded turquoise, the neurotrophins (NT3, BDNF, NGF, TrkB, TrkC), the insulin/IGF family (IGF1, IGF1R, IGF2R, insulin receptor), and PDGFs (PDGFA, PDGFB, PDGFC, PDGFRβ). Intriguingly, some unanticipated ligand/receptor families were also co-expressed in this cluster, including IFNγ (IFNγ, IFNγRα, IFNγRβ) and the GDNF family (GDNF, persephin, GFRα1, GFRα2, GFRα4, Ret).

Cell-Surface Proteomics to Refine the Cortical Precursor and Neuron Communication Model

One disadvantage of a transcriptome-based model is that the correlation between mRNA abundance and protein expression levels is weaker for cell-surface proteins such as growth factor receptors than for proteins in other compartments (Lundberg et al., 2010). We therefore characterized the cell-surface proteome of cortical neurons and enriched precursors. To do this, we performed periodate oxidation of cell-surface glycans on cultured cells using established methods to couple glycosylated proteins to a hydrazide resin (McDonald et al., 2009; Schiess et al., 2009). The coupled, selectively modified glycosylated cell-surface proteins were then tryptically digested, glycopeptides released by PNGase F, and peptides identified by mass

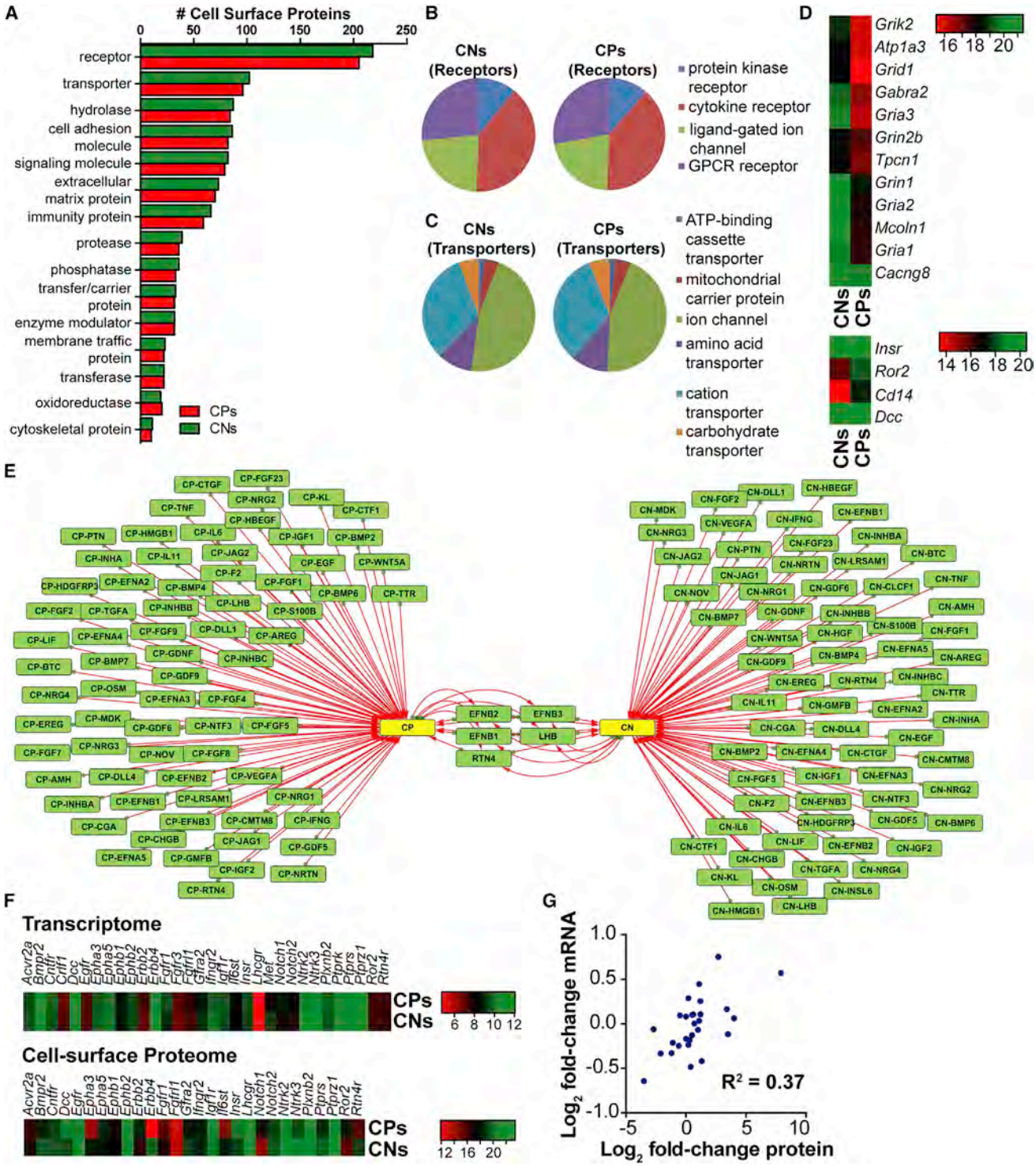

Figure 3. Refining the Growth Factor Communication Network Model by Determining the Cell-Surface Proteome of Cortical Precursors and Neurons

The cell-surface proteome of three replicates each of enriched precursors (CPs) and cortical neurons (CNs) was determined by mass spectrometry of glycosylated membrane-bound proteins.

(A) Number of cell-surface proteins identified in CPs (red) and CNs (green) classified by PANTHER protein class GO analysis.

(B and C) Pie charts of different receptor (B) and transporter (C) subclasses determined as in (A).

(legend continued on next page)

spectrometry. For each sample, we analyzed three independent biological replicates. This analysis identified 1,506 and 1,571 proteins on cortical neurons and precursors, respectively (Table S6). GO analysis of these proteins using PANTHER identified high enrichment for terms associated with the exterior of cells/vesicles as well as membrane-bound components as expected for cell-surface proteins (Figure S2A; Table S7). Further analysis using PANTHER classified, in both neurons and precursors, over 200 proteins as receptors, and about 100 as transporters (Figure 3A; Table S8). Other major categories included cell adhesion molecules, extracellular matrix proteins, and signaling proteins (Figure 3A; Table S8).

PANTHER analysis also identified four major receptor categories with similar proportions in both cell populations: protein kinase receptors, cytokine receptors, ligand-gated ion channels, and G protein-coupled receptors (Figure 3B; Table S9). Transporters fell into three major subcategories that were equally represented in both populations: ion channels, cation transporters, and amino acid transporters (Figure 3C; Table S9). The similarities between neurons and precursors extended to other cell-surface proteins such as cell adhesion molecules and extracellular matrix proteins. However, some proteins were highly enriched in one or the other population. For example, many neurotransmitter receptors and ion channels, including multiple glutamate receptors, were enriched in neurons, while the insulin receptor, the netrin receptor DCC, and the tyrosine-protein kinase receptor ROR2 were enriched in precursors (Figure 3D).

We integrated the cell-surface proteome data with our transcriptome-based communication model by identifying receptors for ligands in the transcriptome model and overlapping them with those from the proteomic data (Figure 3E; Figure S2B). This verified 32 receptors and 86 of 292 potential ligands in the transcriptome-based model. Most of these receptors were present on both populations, with the exception of Met and FGFR3, which were only detectable on neurons and enriched precursors, respectively. A comparison of the relative expression of the 32 validated receptors demonstrated a positive correlation between the $\log_2$ fold-changes computed from the proteome versus the transcriptome data (Figures 3F and 3G), supporting the quantitative nature of this combined approach.

The Cortical Communication Model Identifies Potential In Vivo Interactions

To validate our communication model in vivo, we first asked whether the predicted ligands were expressed in the embryonic cortex, comparing them to the ligand mRNAs expressed at levels greater than or equal to FGF2 mRNA in previously published E13/14 cortex microarray data (Kusek et al., 2012; GEO: GSE38222). We chose this as our cut-off, since FGF2 is expressed in and functionally relevant for the E13/14 cortex (Raballo et al., 2000). 263 growth factor mRNAs were expressed in the cortex at this age (Table S10), and 86% (227 of 263) of these were predicted in the transcriptome model (Figure 4A).

We also used Spearman rank correlation to compare relative ligand mRNA expression in E13/14 cortex, cortical neurons, and enriched precursors. This analysis (Figure 4B) showed high correlations between all three groups. In contrast, there were low correlations between these groups and microglia ligand mRNAs expressed at levels higher than or equal to FGF2 that were extracted from previously published microarrays (Nomaru et al., 2014; GEO: GSE40714). A statistical analysis by pairwise comparison demonstrated $-\log_{10}$-transformed and Bonferroni corrected p values between 33.8 and 35.6 for E13/14 cortex versus precursors and neurons, respectively, and of only 2.2 to 6.6 for microglia versus precursors and neurons (Figure S3A). As an additional control, we randomized the relative ligand orders. All of the Spearman rank correlations and their pairwise comparisons yielded values near zero (Figure S3B).

We next overlaid the E13/14 cortex ligands on the communication models. This refinement removed 52 ligands from the transcriptome-based communication network, but the large majority of the predicted interactions were maintained (Figure 4C). In the transcriptome plus proteome-based network (Figure 4D), 67 of 75 potential ligands were validated. Thus, the cultured neurons and enriched precursors were predictive of the in vivo environment.

One final potential caveat with this analysis is the relatively low percentage of intermediate progenitors in our precursor cultures versus the E13/14 cortex (5%–9% versus about 10%–20%, respectively). To ask whether this would impact our communication model, we extracted differentially expressed ligands and receptors from microarray data of the E14.5 cortex with or without intermediate progenitors due to conditional knockout of the Tbr2 gene (*Nestin-Cre*; $EOMES^{fl/fl}$ mice; Elsen et al., 2013; GEO: GSE43387). Only three ligand and two receptor mRNAs were differentially expressed ($p < 0.05$ FDR) in the cortex without intermediate progenitors: *Adcyap1* (2.8-fold increased), *Angpt1* (4.2-fold increased), *Fstl5* (1.6-fold increased), *Sstr2* (0.5-fold decreased), and *Nrp2* (1.8-fold increased). These ligands are included in our model, and these changes would have no impact on their inclusion.

Identification of Proneurogenic Factors Based on the Cortical Communication Model

We tested our refined communication model, asking whether it could predict ligands that regulate neurogenesis by focusing

(D) Heatmap of average $\log_2$ levels of neurotransmitter receptors enriched in CNs (top) and growth factor receptors enriched in CPs (bottom), as determined from label-free mass spectrometry quantification.

(E) An integrated transcriptome-cell-surface proteome cortical communication network model integrating the transcriptome model in Figure 2F with the cell-surface proteomic data. All green nodes represent ligands that have receptors identified by cell-surface proteomics in CPs or CNs. Nodes surrounding the yellow CP and CN nodes represent predicted autocrine ligands for CPs and CNs, respectively. Nodes located between the yellow CP and CN nodes are predicted paracrine ligands. Edges indicate direction of communication.

(F and G) Differential expression of 32 CP and CN receptors from the integrated model, comparing the transcriptome and proteome data. (F) Heatmaps of $\log_2$ average expression data. Met and FGFR3 are not included in the Cell-surface Proteome heatmap, since they were only detected in neurons and precursors, respectively. (G) Correlation between the $\log_2$ fold-changes at the mRNA versus protein level. Also see Figure S2.

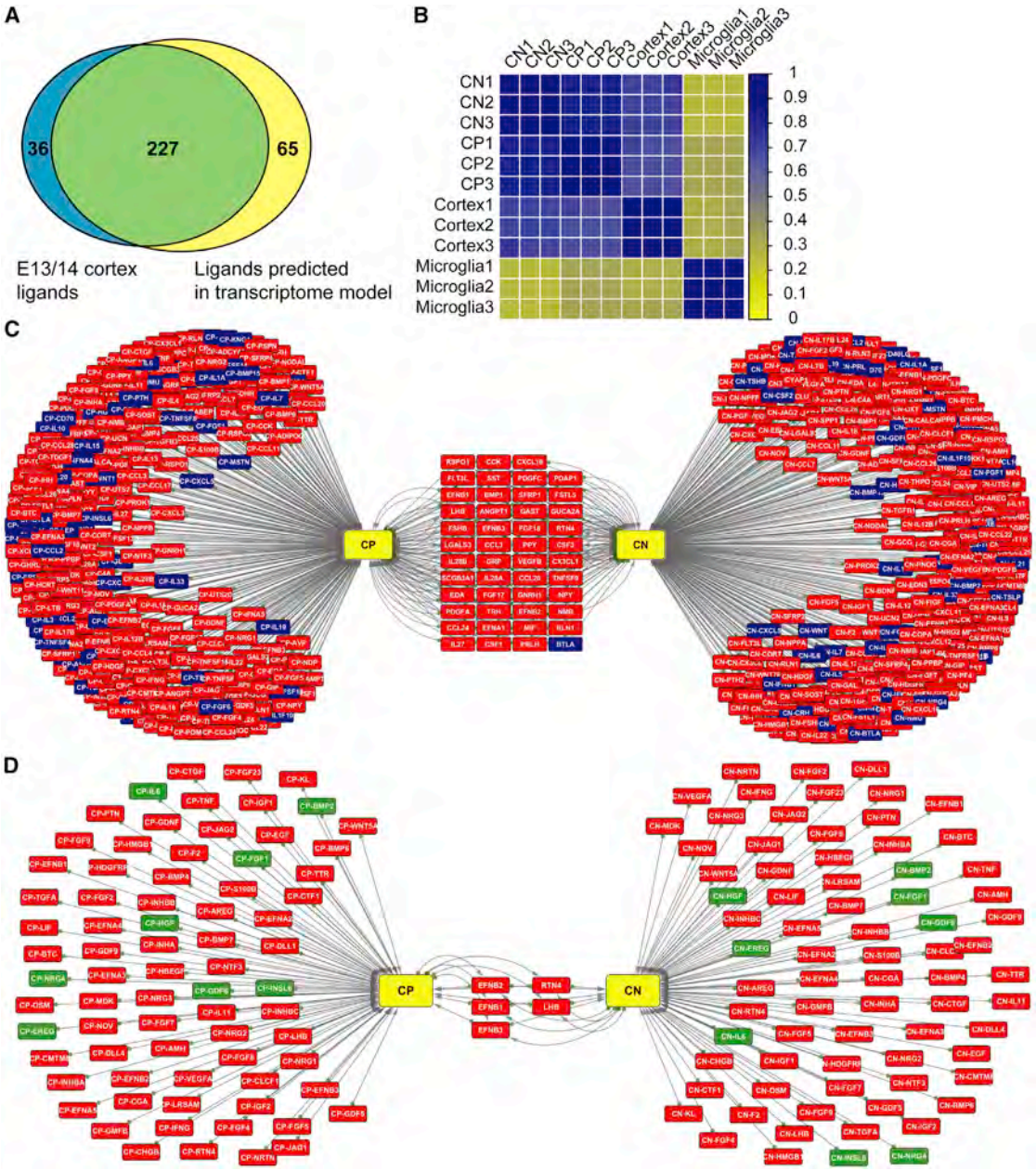

Figure 4. The Cortical Communication Model Predicts Ligands Expressed in the E13/14 Cortex

(A) Venn diagram showing overlap between the 292 ligands from the transcriptome-based model, and the 263 ligand mRNAs expressed at levels ≥FGF2 mRNA in the E13/14 cortex (determined from GSM936937, GSM936940, and GSM936943 from Kusek et al., 2012).

(B) Spearman rank correlation of ligand mRNAs expressed by cultured cortical neurons (CN1–CN3), enriched precursors (CP1–CP3), E13/14 cortex (Cortex1–Cortex3), and purified microglia (Microglia1–Microglia3, extracted from GSM999630, GSM999631, and GSM999632 from Nomaru et al., 2014).

(C and D) Integration of the E13/14 cortex ligand data with the transcriptome-based cortical communication model in Figure 2F (C) and the combined transcriptome-cell-surface proteome communication model shown in Figure 3E (D). Red nodes in (C) denote ligands predicted in the transcriptome-based model that were also expressed in the E13/14 cortex, while those in (D) also have receptors identified by cell-surface proteomics. In both models, nodes surrounding the yellow CP and CN nodes represent predicted autocrine ligands for CPs and CNs, respectively. Nodes located between the yellow CP and CN nodes are predicted paracrine ligands. Edges indicate direction of communication. Also see Figure S3.

on 15 ligands expressed in E13/14 cortex (Figures 4C and 4D; Table S10) but not previously characterized in this context. We examined eight ligands predicted by the integrated transcriptomic/proteomic model (Figure 5A) and seven predicted by the transcriptome model alone (Figure 5B). We plated E13 precursors in 96-well plates (50,000 cells/cm^2) and added individual ligands at 100 ng/mL for 3 days. Immunostaining for βIII-tubulin and high-content image analysis (Figures 5C and 5D) showed

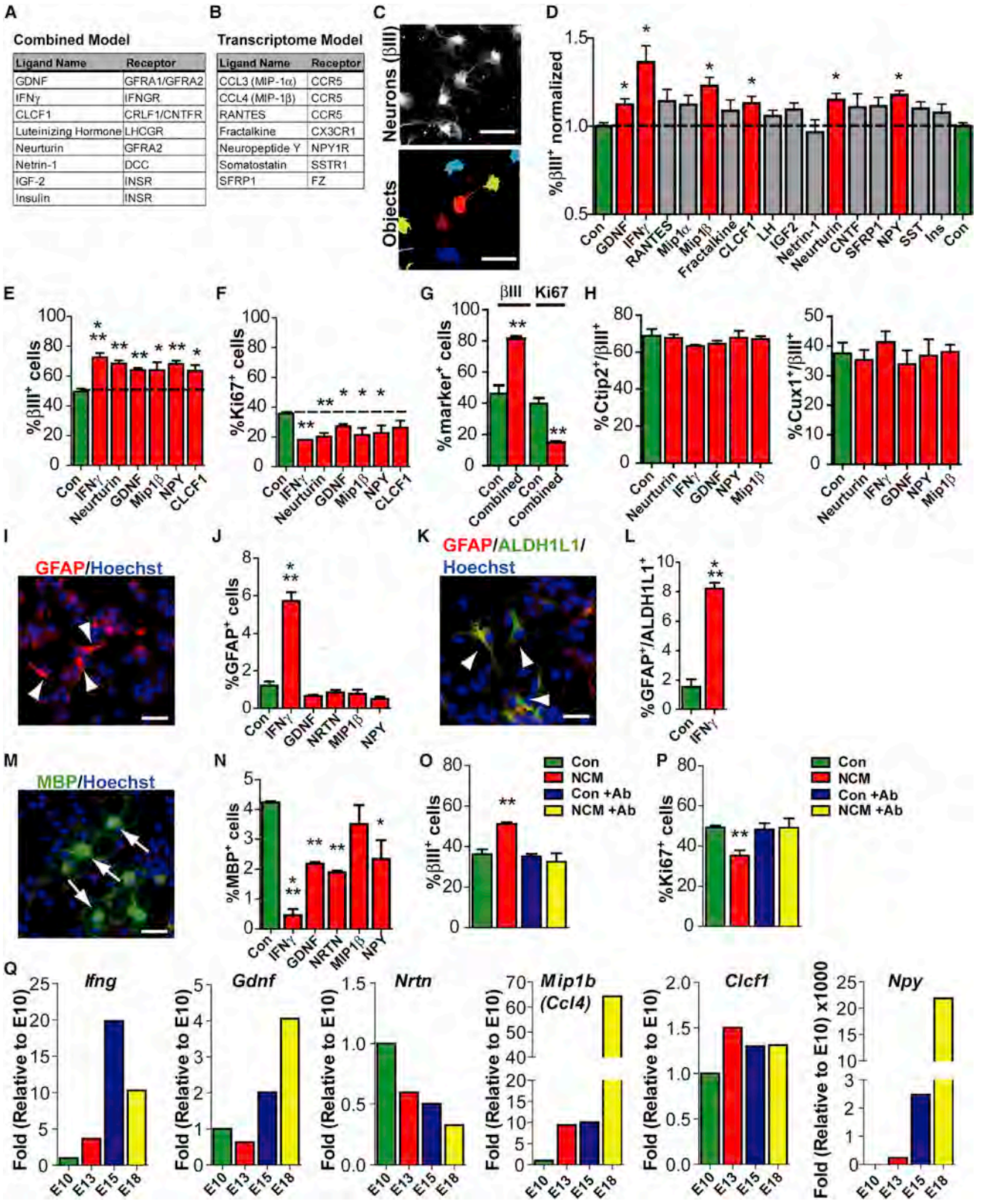

(legend on next page)

that six ligands significantly increased newborn neurons: GDNF, Nrtn, macrophage inflammatory protein 1β (Mip1β, or CCL4), cardiotrophin-like cytokine factor 1 (CLCF1), IFNγ, and neuropeptide Y (NPY).

We validated these results by adding these ligands individually or together in similar culture experiments and manually counting cells positive for βIII-tubulin and Ki67. All six individual factors enhanced neurogenesis (Figure 5E) and, with the exception of CLCF1, significantly decreased Ki67-positive proliferating precursors (Figure 5F). Moreover, the combined factors almost doubled βIII-tubulin-positive neurons, and decreased proliferating precursors by almost 3-fold, an effect greater than that with any individual factors (Figure 5G). Of the six validated ligands, four were from the combined transcriptome/proteome model.

We further characterized five of the ligands, omitting CLCF1 since it had the most modest effects (Figures 5E and 5F). First, we asked whether they preferentially or differentially affected cortical neuron phenotypes when added to E13 precursors for 3 days. Immunostaining for βIII-tubulin and Cux1, which marks later-born, superficial neurons, or Ctip2, which marks deeper layer neurons showed that with and without added ligands, approximately 60% and 40% of neurons expressed Ctip2 and Cux1, respectively (Figure 5H). Second, we asked whether they affected gliogenesis when added to E13 precursors for 7 days. Immunostaining showed that in control cultures, about 1.5% of cells expressed the astrocyte marker GFAP, and only IFNγ had any effect, increasing it to about 6% (Figures 5I and 5J). We confirmed that these GFAP-positive cells were likely to be astrocytes by colabeling them for a second astrocyte marker, ALDH1L1 (Figures 5K and 5L). We also assessed oligodendrogenesis by immunostaining similar cultures for MBP (Figure 5M). Under control conditions, about 4% of cells were MBP positive, and this was significantly decreased by all ligands except Mip1β (Figure 5N). Thus, four of the ligands selectively enhanced neurogenesis, while IFNγ also promoted astrogenesis.

Since our transcriptome data indicated that all five of these ligands were expressed by cortical neurons, we asked whether they were responsible for the proneurogenic effects of neuron-conditioned medium. To test this idea, we cultured E13 precursors with neuron-conditioned medium in the presence of previously validated neutralizing antibodies toward GDNF, Nrtn, IFNγ, and Mip1β together with an NPY receptor (NPYR) antagonist. As a control, we used an equal concentration of non-specific IgG. Immunostaining 3 days later showed that neuron-conditioned medium enhanced neurons and decreased precursors and that the function-blocking antibody mixture abrogated these effects (Figures 5O and 5P). Thus, at least one of the five ligands is secreted by neurons to promote neurogenesis in culture.

The Proneurogenic Ligands Promote Differentiation of Radial Precursors into Intermediate Progenitors and Neurons In Vivo

To validate these ligands in vivo, we first confirmed their expression by qRT-PCR. All five ligand mRNAs were expressed in the cortex from E10 to E18, with differing profiles (Figure 5Q). *Nrtn* and *Clcf1* mRNAs were relatively constant, *Gdnf* and *Ifng* mRNA levels increased several-fold from E13 to E15, while *Mip1b* and *Npy* mRNA levels were low at E13 and E15 with large increases during late embryogenesis.

We asked whether these ligands could promote neurogenesis in vivo, taking advantage of the fact that the apical endfeet of cortical radial precursors are adjacent to the lateral ventricles. We therefore injected a mixture of Nrtn, GDNF, IFNγ, MIP1β, and NPY into the lateral ventricles of E13/14 mouse embryos in utero to increase their concentrations locally. At the same time, we injected the mothers with BrdU to assess proliferation. Two days later, we immunostained embryonic cortical sections for BrdU and the intermediate progenitor marker Tbr2, or SatB2, which labels almost all neurons born during this time period (Gallagher et al., 2013) (Figures 6A and 6B; Figure S4A). The combined ligands doubled BrdU-positive, Tbr2-positive intermediate progenitors and significantly increased BrdU-positive, SatB2-positive neurons relative to control injections (Figure 6C). Immunostaining for BrdU and Pax6 or Ki67 showed that BrdU-positive, Pax6-positive, or Ki67-positive precursors were concomitantly decreased (Figures 6D–6G; Figure S4A).

IFNγ, Nrtn, and GDNF Are Required for Normal Cortical Neurogenesis In Vivo

These data show that the combined ligands promoted neurogenic differentiation of radial precursor cells in vivo. We therefore asked whether the endogenous ligands were important for

Figure 5. Ligands Predicted by the Integrated Communication Model Promote Neurogenesis in Culture

(A and B) Ligands chosen for further analysis that were predicted by (A) the integrated transcriptome-proteome communication model in Figure 4D or (B) the transcriptome only model in Figure 4C.

(C and D) 100 ng/mL of the selected ligands were added individually to E13 precursors, and cultures were immunostained 3 days later for βIII-tubulin and analyzed by high-content image analysis using CellProfiler. (C) shows βIII-tubulin immunostaining (top) and the objects identified in this image as neurons by CellProfiler (bottom; different colors are different objects), and (D) shows quantification, normalized to controls without ligands. *$p < 0.05$ (Student's unpaired t test with FDR correction for multiple comparisons), n = 4 experiments.

(E–H) 100 ng/mL of proneurogenic ligands were added alone (E, F, and H) or together (G) to cultured E13 precursors, and βIII-tubulin-positive neurons (E and G), Ki67-positive precursors (F and G), or βIII-tubulin-positive neurons coexpressing Cux1 or Ctip2 (H) were determined by immunostaining and counting manually. *$p < 0.05$, **$p < 0.01$, ***$p < 0.001$, n = 3–4 experiments.

(I–N) Precursors were cultured with 100 ng/mL IFNγ, Nrtn, GDNF, MIP1β, or NPY for 7 days, immunostained for GFAP (red, I,K), ALDH1L1 (green, K) or MBP (green, M), and quantified for single-positive (J and N) or double-positive (L) cells. *$p < 0.05$, **$p < 0.01$, ***$p < 0.001$, n = 3 experiments.

(O and P) Quantification of βIII-tubulin-positive neurons (O) or Ki67-positive precursors (P) from E13 precursors cultured with control IgG in control medium (Con) or neuron-conditioned medium (NCM), or with a function-blocking antibody mixture in control medium (Con+Ab) or neuron-conditioned medium (NCM+Ab). **$p < 0.01$, n = 3 experiments.

(Q) qRT-PCR for *Nrtn*, *Gdnf*, *Ifng*, *Npy*, *Clcf1*, and *Mip1b* mRNAs in E10, E13, E15, and E18 cortices. Levels were normalized to *Gapdh* and expressed as fold-change relative to E10. Scale bars represent 25 μm. Error bars represent SEM.

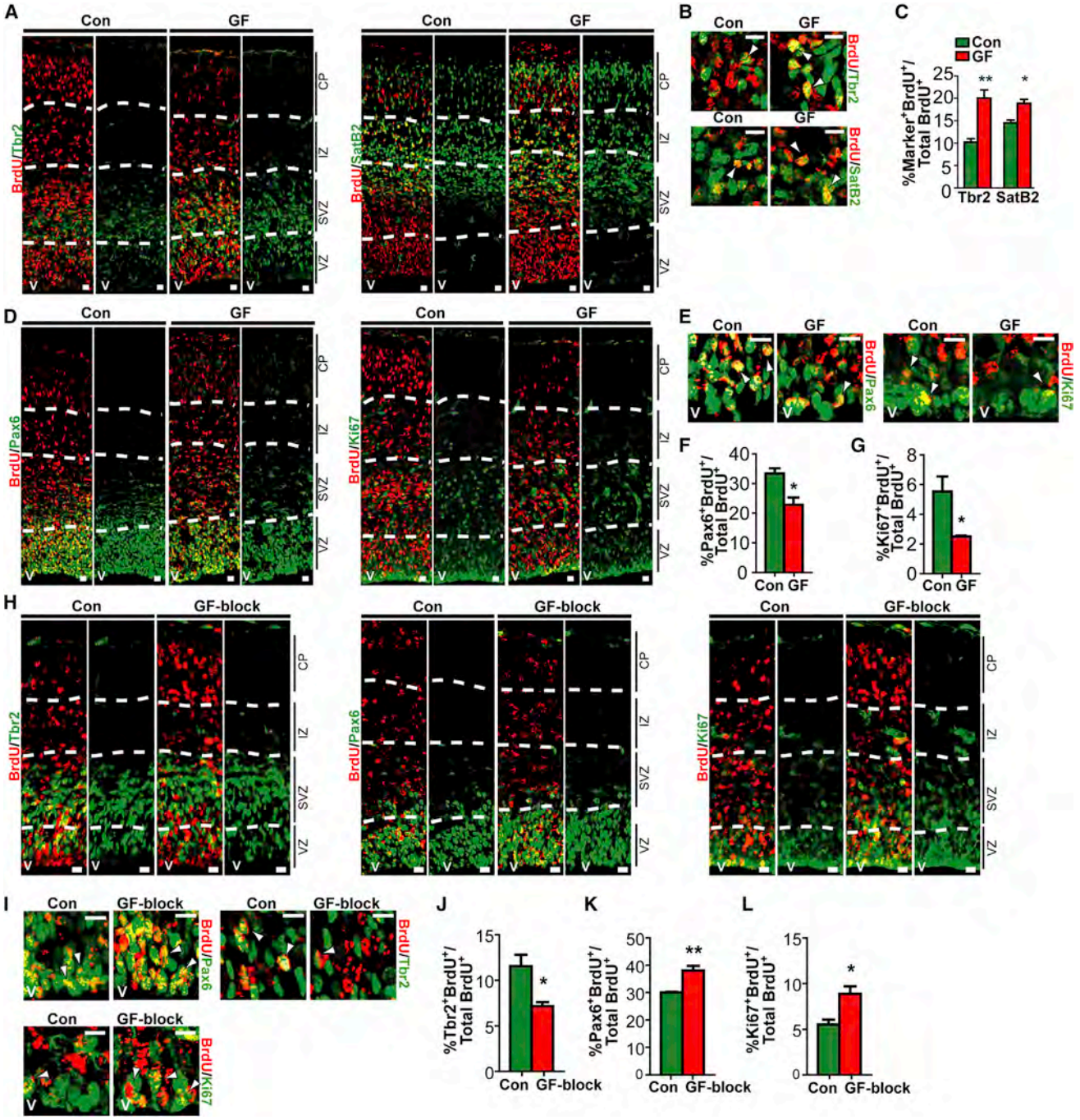

Figure 6. Nrtn, GDNF, and IFNγ Are Necessary for Cortical Neurogenesis In Vivo

A combination of Nrtn, GDNF, IFNγ, MIP1β, and NPY (GF) or vehicle (Con) (A–G) or function blocking antibodies toward Nrtn, GDNF, IFNγ, MIP1β, and a receptor antagonist toward NPYR (GF-block) or an equal amount of non-specific IgG (Con) (H–L) were injected into the lateral ventricles of E13/14 embryos coincident with maternal BrdU injection. Two days later, coronal cortical sections were immunostained for BrdU (red in all images) and Tbr2 (green, A, B, H, and I), Satb2 (green, A and B), Pax6 (green, D, E, H, and I), or Ki67 (green, D, E, H, and I) and quantified for the proportion of total BrdU-positive cells that were also positive for these markers (C, F, G, and J–L). Low-magnification images (A, D, and H) show the marker alone and the merged image with BrdU. High-magnification images of Tbr2 (B and I), SatB2 (B), and Pax6 and Ki67 (E and I) show the SVZ, cortical plate, and VZ/SVZ, respectively. In all images, arrowheads denote double-labeled cells. *$p < 0.05$, **$p < 0.01$, $n = 9$ sections each (3 each from 3 embryos, all from independent mothers). Scale bars represent 25 μm in (A), (D), and (H) and 10 μm in (B), (E), and (I). Error bars represent SEM. Also see Figure S4.

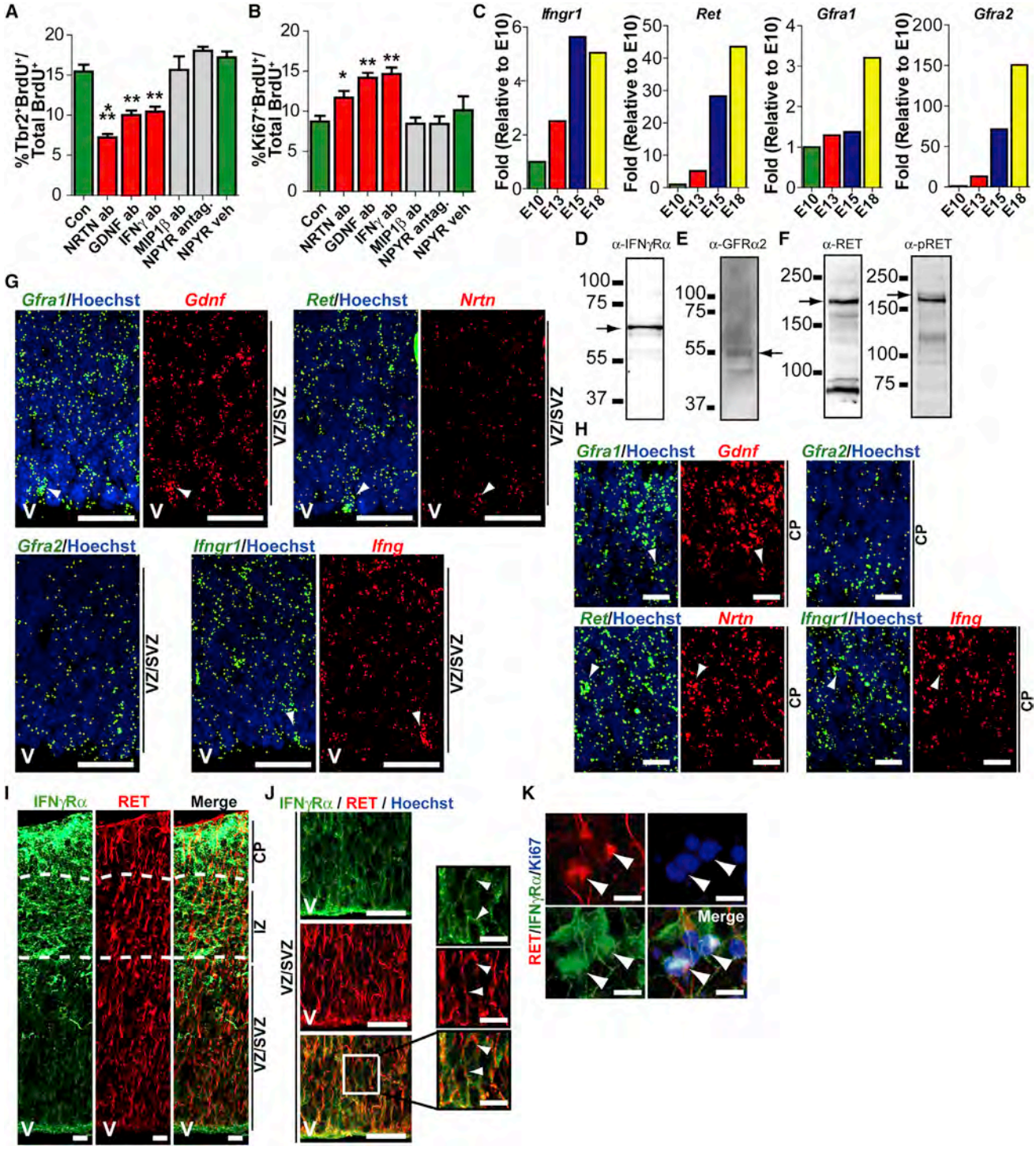

Figure 7. Expression of Nrtn, GDNF, IFNγ and Their Receptors in the Embryonic Cortex

(A and B) Individual function blocking antibodies toward Nrtn, GDNF, IFNγ, MIP1β, or the NPYR antagonist were injected into E13/14 lateral ventricles, coincident with maternal BrdU injection. As controls, ventricles were injected with an equal amount of non-specific IgG (Con) or vehicle (NPYR veh). Two days later, sections were immunostained and quantified for BrdU-positive cells expressing Tbr2 (A) or Ki67 (B). *p < 0.05, **p < 0.01, ***p < 0.001, n = 3–5 embryos, 3 sections per embryo.

(C) qRT-PCR analysis of *Gfra1*, *Gfra2*, *Ret*, and *Ifngr1* mRNAs in E10, E13, E15, and E18 cortices. Levels were normalized to *Gapdh* and expressed as fold-change relative to E10.

(legend continued on next page)

neurogenesis by injecting the lateral ventricles of E13/14 embryos with function-blocking antibodies for Nrtn, GDNF, IFNγ, MIP1β, and the NPY receptor antagonist. We coincidentally injected the mothers with BrdU. We confirmed that injected antibodies penetrated the cortical tissue by injecting non-specific goat IgG and immunostaining embryonic cortical sections 2 days later with an appropriate secondary antibody (Figure S4B). We also directly labeled the Nrtn antibody with an Alexa Fluor 555 tag and showed that 6 hr after injection into the lateral ventricles, it was found throughout the cortical tissue (Figure S4C).

Having validated this approach, we asked whether function-blocking antibodies affected neurogenesis. Immunostaining 2 days post-injection (Figures 6H and 6I; Figure S4D) showed that, relative to control IgG, the function-blocking antibodies significantly decreased BrdU-positive, Tbr2-positive intermediate progenitors and increased the proportion of BrdU-positive, Pax6-positive radial precursors and Ki67-positive proliferating precursors (Figures 6J–6L). We asked which of the function-blocking antibodies mediated this effect, performing similar experiments with single antibodies or the NPY receptor antagonist. Immunostaining 2 days post-injection showed that the antibodies to Nrtn, GDNF, and IFNγ all significantly decreased BrdU-positive, Tbr2-positive intermediate progenitors and increased BrdU-positive, Ki67-positive proliferating precursors (Figures 7A and 7B). In contrast, the MIP1β antibody and the NPY receptor antagonist had no effect on either parameter (Figures 7A and 7B). Thus, the three proneurogenic ligands predicted by the combined transcriptome/proteome model, but not the two predicted only at the transcriptome level, were necessary for neurogenesis in vivo.

IFNγ, Nrtn, and GDNF and Their Receptors Are Expressed in Radial Precursors and Newborn Cortical Neurons in the Embryonic Cortex

These data indicate that GDNF, Nrtn, and IFNγ are important for appropriate genesis of intermediate progenitors and neurons. We further characterized expression of these ligands and their receptors using a number of approaches. First, qRT-PCR showed that the mRNAs encoding the relevant receptors, *Gfra1*, *Gfra2*, *Ret*, and *Ifngr1*, increased in expression in the cortex from E10 to E18 (Figure 7C). Second, western blots showed that IFNγRα, GFRα2, and Ret were all expressed at the protein level in the E13 cortex and that Ret was present in its phosphorylated, activated form (Figure 7D), consistent with the presence of GDNF family ligands. Third, we performed single-molecule fluorescence in situ hybridization (FISH) on sections of E12, E15, and E17 cortices (Figures 7G and 7H; Figures S5A–S5E). This analysis demonstrated low but detectable expression of *Gdnf*, *Nrtn*, *Ifng*, *Ret*, *Gfra1*, *Gfra2*, and *Ifngr1* mRNAs throughout the E12 cortex (Figures S5A and S5B). At E15 and E17, their expression (except for *Nrtn* mRNA) was apparently increased, and all were present in both the VZ/SVZ precursor zones and the cortical plate (Figure S5C). High-magnification double-label FISH at E15 showed readily detectable expression of all mRNAs in radial precursors in the apical VZ (Figure 7G), and neurons in the cortical plate (Figure 7H). This analysis also showed that the ligand and receptor mRNAs (*Gfra1* and *Gdnf*, *Ret* and *Nrtn*, *Ifng* and *Ifngr1*) were expressed in the same and/or adjacent cells in these regions (Figures 7G and 7H). Similar results were obtained at E17 (Figures S5D and S5E).

Finally, we immunostained the E13 cortex for IFNγRα and Ret (Figures 7I and 7J). Both IFNγRα and Ret were present throughout the cortex, and many cells in the VZ/SVZ were positive for both receptors. Immunostaining of E13 cultures confirmed this localization, showing that most Ki67-positive precursors were also positive for Ret and IFNγRα (Figure 7K).

The GDNF/Nrtn Coreceptor Ret and IFNγRα Are Necessary for Normal Cortical Neurogenesis

These data suggest that GDNF, Nrtn, and IFNγ act directly on radial precursors to regulate neurogenesis. To test this idea, we generated shRNAs for their receptors IFNγRα and Ret, confirming their efficacy in HEK293 cells cotransfected with expression constructs for the relevant receptors (Figures 8A and 8B). We also tested the two most efficacious of these shRNAs, shIFNGR1A and shRET2, in cultured E13 precursors, cotransfecting them with an EGFP expression vector. Immunostaining and image analysis 3 days later showed that Ret and IFNγRα immunofluorescence were significantly reduced in cells transfected with the relevant shRNA (Figures 8C and 8D).

We used these shRNAs to knock down receptor expression in apically localized radial precursors in vivo using in utero electroporation (Gauthier-Fisher et al., 2009). We first electroporated E13/14 cortices with control or Ret shRNAs together with a nuclear EGFP expression vector. Immunostaining of cortical sections 2 days post-electroporation showed that both shRET1 and shRET2 altered cellular distribution, with more EGFP-positive cells in the VZ and fewer in the SVZ and cortical plate relative to a control shRNA (Figures 8E and 8F). This change in distribution was likely due to decreased neurogenesis, since Ret knockdown significantly decreased EGFP-positive, Tbr2-positive intermediate progenitors and increased proliferating radial precursors, as indicated by immunostaining for EGFP and Pax6 or Ki67 (Figures 8G–8J).

We performed similar experiments to knock down IFNγRα. Immunostaining 2 days post-electroporation showed that both

(D–F) Western blots of total protein from E13 cortices probed for IFNγRα (D, arrow), GFRα2 (E, arrow), Ret (F, left panel, arrow), and the phosphorylated, activated Ret receptor (pRET) (F, right panel, arrow). Size bars indicate molecular weight markers in kDa.

(G and H) High-magnification images of the E15 VZ/SVZ (G) or cortical plate (H), showing double-label FISH for *Gfra1* mRNA (green) and *Gdnf* mRNA (red), for *Ret* mRNA (green) and *Nrtn* mRNA (red), for *Ifngr1* mRNA (green) and *Ifng* (red), and for *Gfra2* mRNA (green). Each pair shows the same field, with Hoechst 33258 (blue) colabelling of the left image. Arrowheads indicate double-labeled cells.

(I and J) Images of E13 cortex double labeled for IFNγRα (green) and Ret (red). (I) shows the entire cortex at lower magnification, and (J) shows the VZ/SVZ, with the boxed area shown at higher magnification to the right. Arrowheads indicate double-labeled cells.

(K) E13 precursors cultured 3 days, and triple-labeled for Ret (red), IFNγRα (green), and Ki67 (blue). Arrowheads denote triple-labeled cells. Error bars indicate SEM. Scale bars represent 25 μm in (G)–(J) or 10 μm in inset of (J) and (K). Also see Figure S5.

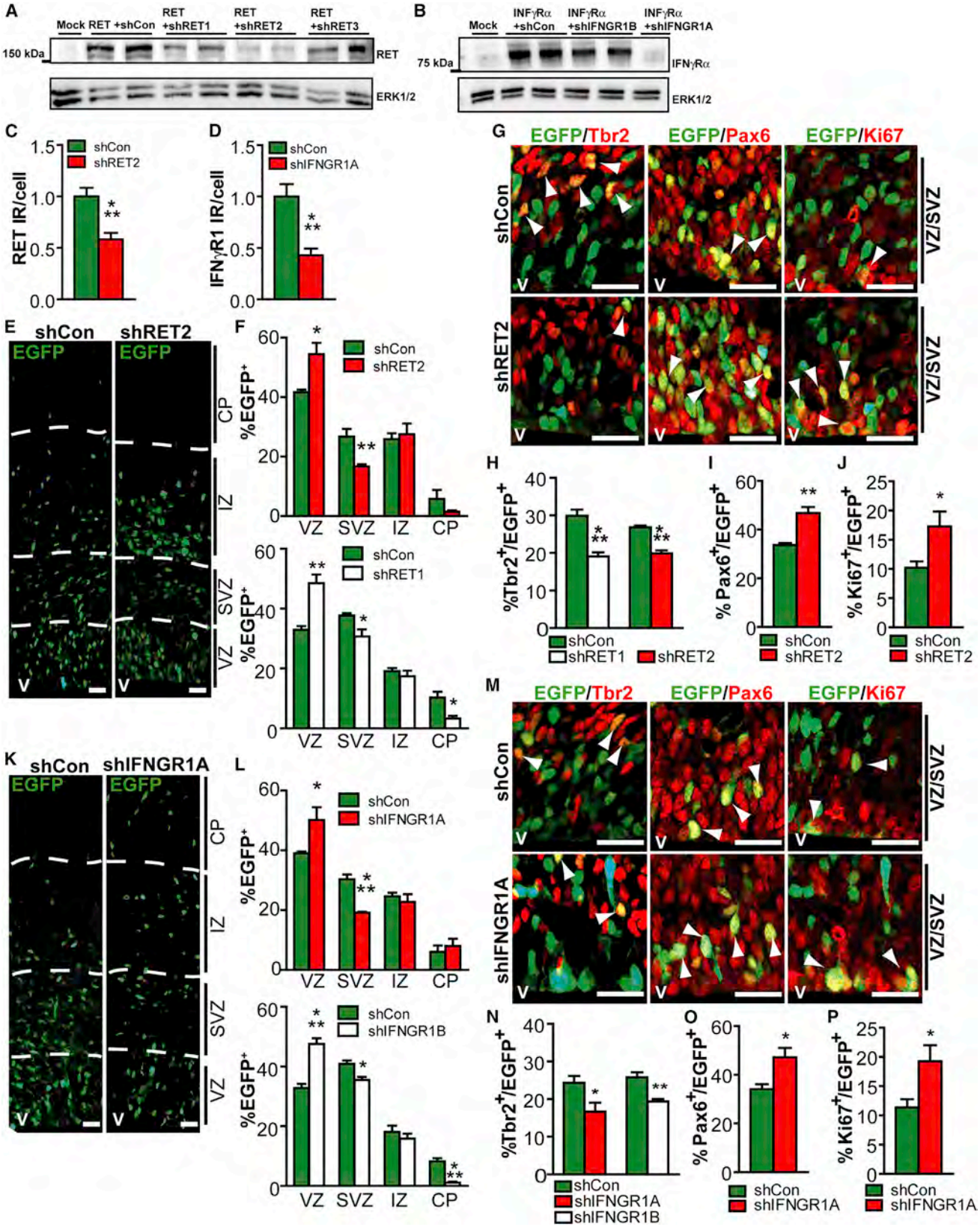

(legend on next page)

shIFNGR1A and shIFNGR1B increased EGFP-positive cells in the VZ and decreased those in the SVZ relative to the control shRNA (Figures 8K and 8L). Moreover, EGFP-positive, Tbr2-positive intermediate progenitors were decreased by both shRNAs (Figures 8M and 8N) and EGFP-positive, Pax6-positive radial precursors and EGFP-positive, Ki67-positive proliferating precursors were increased following shIFNGR1A-mediated knockdown (Figures 8M, 8O, and 8P). Thus, consistent with the requirement for GDNF, Nrtn, and IFNγ shown by the function-blocking antibody experiments, both Ret and IFNγRα are required for radial precursors to undergo appropriate levels of neurogenic differentiation.

DISCUSSION

In this study, we used an iterative systems biology approach to generate a growth factor communication network within and between embryonic cortical radial precursors and their newborn neuronal progeny, and based on this model, identified growth factors that regulate cortical neurogenesis in vivo. Our work supports a number of broad conclusions about these embryonic cortex growth factor interactions. First, we show that cortical precursors secrete factors that promote their own self-renewal/proliferation, while cortical neurons secrete factors that promote neurogenesis. These findings make good biological sense. At early stages, precursors are the predominant cell type and the cortical microenvironment would be enriched in growth factors that promote proliferation and thus expansion of the cortex. As radial precursors start to generate neurons, the microenvironment would become enriched in proneurogenic factors that would enhance neurogenesis, and perhaps even initiate genesis of neurogenic intermediate progenitors, as we show here for IFNγ, Nrtn, and GDNF.

Second, our communications model predicts a complex cortical growth factor environment with many previously uncharacterized autocrine and paracrine interactions. This complexity would not have been appreciated by traditional candidate factor analyses and may explain the diversity of NPC responses observed when analyzing single ligands in isolation (Gauthier-Fisher and Miller, 2013). This complexity might also reflect an unexpected heterogeneity within the cortical radial precursor pool, with subsets of precursors responding selectively to different environmental cues. Third, this same model predicted a large number of factors not previously considered in the embryonic cortex, three of which, IFNγ, Nrtn, and GDNF, we validated as regulators of cortical neurogenesis. Many of these "new" ligands and receptors are predicted to be shared by precursors and neurons, suggesting that the same ligand-receptor pairs might sequentially regulate different aspects of cortical development. For example, previous work showed that the GDNF family regulates migration of cortical interneurons and excitatory neurons (Lundgren et al., 2012; Pozas and Ibáñez, 2005) and our data show that this family also directly regulates neurogenesis itself.

Finally, our data imply that the ultimate cortical precursor decision to self-renew or differentiate is likely determined by multiple, convergent growth factor inputs. We propose that this convergence occurs, at least in part, at the intracellular level, as exemplified by the proneurogenic factors we identified here. GDNF and Nrtn bind to their preferred receptors, GFRα1 and GFRα2, respectively (Jing et al., 1997) and these ligand-coreceptor complexes associate with Ret, causing transphosphorylation of Ret and activation of downstream signaling pathways, including the MEK-ERK pathway (Worby et al., 1996). IFNγ binds to the high-affinity IFNγRα chain, inducing receptor oligomerization with the IFNγRβ chain (Igarashi et al., 1994) and activating several downstream pathways, including the MEK-ERK pathway (Roy et al., 2002). Intriguingly, we previously showed that a MEK-ERK-C/EBP pathway is essential for cortical neurogenesis (Ménard et al., 2002), providing one convergent proneurogenic pathway that all of these ligands would activate.

Systems-level and network analyses are now being applied to diverse areas of neuroscience (Parikshak et al., 2015), including, for example, autism spectrum disorder (Parikshak et al., 2013) and neural cell heterogeneity (Zeisel et al., 2015). However, systems-level techniques are just now being applied to cell-cell communication, largely within the hematopoietic/immune system (Kirouac et al., 2010; Qiao et al., 2014). Here, we have applied these approaches to obtain a broad overview of the growth factor environment in the developing cortex. Ongoing work connecting our cell interaction networks to spatially resolved single-cell analysis will ultimately allow us to understand how precursors and neurons integrate a wide variety of exogenous signals during normal and abnormal brain development.

EXPERIMENTAL PROCEDURES

Animals and Reagents

All animal use was approved by the HSC Animal Care Committee in accordance with CCAC policies. CD1 mice (Charles River Laboratory) were used

Figure 8. Ret and IFNγRα Are Necessary for Radial Precursors to Differentiate along the Neurogenic Pathway In Vivo

(A and B) Western blots of total protein from HEK293 cells cotransfected with murine Ret (A) or IFNγRα (B) expression plasmids and murine Ret shRNAs (A, shRET1, 2 and 3), murine IFNγRα shRNAs (B, shIFNGR1A and shIFNGR1B), or a control shRNA (shCon). The blots were probed for Ret or IFNγRα (top panels) and reprobed for ERK1/2 as a loading control (bottom panels). Mock refers to cells that were not transfected.

(C and D) Cultured precursors were cotransfected with EGFP and shRET2, shIFNGR1A, or a control shRNA (shCon), immunostained after 3 days for EGFP and Ret or IFNγRα, and the relative level of Ret (C) or IFNγRα (D) immunoreactivity was quantified in individual EGFP-positive cells using ImageJ and expressed relative to control shRNA-transfected cells. ***$p < 0.001$, $n = 25$ EGFP-positive cells each.

(E–P) E13/14 cortices were coelectroporated with nuclear EGFP and control shRNA (Con), Ret shRNAs (E–J, shRET2 or shRET1), or IFNγRα shRNAs (K–P, shIFNGR1A and shIFNGR1B), and coronal sections were immunostained 2 days later. (E, F, K, and L) Sections were immunostained for EGFP (green, E and K), and the relative distribution of EGFP-positive cells was quantified (F and L). White hatched lines in (E) and (K) demarcate cortical regions. *$p < 0.05$, **$p < 0.01$; ***$p < 0.001$, $n = 4$ embryos, 3 sections each. (G and M) Images of the VZ/SVZ immunostained for EGFP (green) and Tbr2, Pax6, or Ki67 (all red). Arrowheads denote double-labeled cells. (H–J, and N–P) Quantification of sections as in (G) and (M) for EGFP-positive cells that also expressed Tbr2 (H and N), Pax6 (I and O), or Ki67 (J and P). *$p < 0.05$, **$p < 0.01$, ***$p < 0.001$, $n = 4$ embryos, 3 sections each. Scale bars represent 25 μm. Error bars indicate SEM.

for all experiments. All plasmids, shRNAs, growth factor, and antibodies are described in the Supplemental Experimental Procedures.

Primary Cultures

E12/13 cortical precursor cultures were prepared and transfected as previously described (Gallagher et al., 2013) with minor modifications. Purified cortical neurons were cultured from E16 cortices and were treated with 0.5 nM cytosine arabinoside (AraC) for 1 day to remove dividing cells. For coculture experiments, E12/13 precursors were plated directly on purified neurons in precursor medium. Conditioned medium was collected from neurons cultured at 90,000 cells/cm^2 for 2 days, or precursors cultured at 110,000 cells/cm^2 for 3 days. Further details are in Supplemental Experimental Procedures.

In Utero Manipulations

In utero electroporation of E13/14 embryos was performed as described (Gauthier-Fisher et al., 2009). A similar approach was used for growth factors and antibodies, injecting 1 μL containing 20 ng/μL of each growth factor and NPY, 40 ng/μL of each neutralizing antibody plus 1 uM BMS193885, 200 ng/μL of single neutralizing antibodies or, as controls, 0.1% BSA, 200 ng/μL nonspecific goat IgG, or PBS. Mothers were injected i.p. with 400 μL of 20 mg/mL bromodeoxyuridine (BrdU) immediately following embryo reimplantation. Further details are in Supplemental Experimental Procedures.

Immunostaining and FISH

Immunostaining was performed essentially as described (Gallagher et al., 2013). FISH was performed using the RNAScope Multiplex Fluorescent Assay kit (Advanced Cell Diagnostics). Images of immunostaining were collected using a Quorom spinning-disk confocal microscope system or a Zeiss Axio Imager M2 system with an X-Cite 120 LED light source and a C11440 Hamamatsu camera. For FISH, z stacks of confocal images were taken with optical slice thickness of 0.2 μm, and projected z stacked images are shown. Further details, FISH probes and antibodies are in Supplemental Experimental Procedures.

Western Blotting

For knockdowns, HEK293 cells were cultured and transfected and western blots were performed essentially as previously described (Gallagher et al., 2013) with minor modifications as described in Supplemental Experimental Procedures.

qRT-PCR

RNA was isolated using the E.Z.N.A. Total RNA Kit I and E.Z.N.A. RNase-Free DNase I Set (Omega Bio-tek). cDNA was synthesized from 500 ng total RNA using RevertAid H Minus M-MulV Reverse Transcriptase (Thermo-Fisher), and qPCR was performed using Lightcycler 480 SYBR Green I Master mix (Roche) on a C1000 Touch Thermal Cycler (Bio-Rad). *Gapdh* mRNA was used as an endogenous control, and reactions were performed in triplicate. Primers are in Supplemental Experimental Procedures.

Microarray Analysis

Total RNA was isolated with the Ambion RiboPure RNA purification kit, analyzed to ensure RNA quality, and cDNA produced from 100 ng total RNA with the Ambion WT kit. 5.5 μg of labeled cDNA was hybridized on to Mouse Gene 2.0 ST arrays using the Affymetrix FS450_0002 hybridization protocol, and scanned using the Affymetrix GeneChip Scanner 3000. Microarray analysis was performed at the HSC TCAG. Microarray data have been deposited in the GEO database under the GSE84482 accession number.

Mass Spectrometry

Cell-surface mass spectrometry was carried out based on published protocols (McDonald et al., 2009; Schiess et al., 2009) and as described in the Supplemental Experimental Procedures. Data were analyzed using PEAK 7.5 software (Bioinformatics Solutions).

Analysis of Microarray and Mass Spectrometry Data

For microarray data, raw probe intensity values were background corrected, normalized, and transformed using the Oligo bioconductor package in R. To calculate differential gene expression, we used the limma bioconductor package to calculate Bayesian statistics and corrected using the Benjamini and Hochberg false discovery rate (FDR) procedure. Annotation was performed using the "mogene20sttranscriptcluster.db" library in R. Heatmaps were prepared in R using the heatmap.2 function on averaged $\log_2$ RMA-normalized or label-free quantitative proteomic data. The cluster analysis was performed using the complete linkage method of a Euclidian distance matrix. GO analysis was performed using the GOstats bioconductor package in R. The gene "universe" in these analyses was all of the mapped keys in the org.Mm.egGO databases. Spearman rank correlation and pairwise statistical analysis were performed using the corrplot package and cor.test function in R. WGCNA analysis was performed with $\log_2$ RMA-normalized data using the WGCNA package with default parameters and a soft-thresholding power of 6. Further details are in Supplemental Experimental Procedures.

PERT Analysis and Network Construction

As previously described (Qiao et al., 2012, 2014), microarray data were preprocessed with PERT to correct ligand/receptor values for changes in a heterogeneous population of cells, and the cell-cell intraction network was constructed with these corrected values as per the flow chart in Figure S1C. For more details, see Supplemental Experimental Procedures.

Statistical Analyses

For single group comparisons, we used two-tailed unpaired Student's t tests and for multi-group comparisons, ANOVA followed by a Dunnett's post hoc analysis. For the high-content analysis, we used two-tailed unpaired Student's t tests corrected by the Benjamini and Hochberg false-discover rate procedure. In all cases, GraphPad Prism (version 5.0.3) was used.

ACCESSION NUMBERS

The accession number for them microarray data reported in this paper is GEO: GSE84482.

SUPPLEMENTAL INFORMATION

Supplemental Information includes Supplemental Experimental Procedures, five figures, and ten tables and can be found with this article online at http://dx.doi.org/10.1016/j.neuron.2016.07.037.

AUTHOR CONTRIBUTIONS

S.A.Y. conceptualized, designed, performed, and analyzed most experiments and co-wrote the paper. G.Y. performed in utero injections and analysis of the resulting data. M.J.B. performed the shRNA characterization. G.C., with S.A.Y., generated the cell interaction network. G.I.C. and S.K.Z. performed and analyzed qRT-PCR and FISH experiments, respectively. P.Z.W. helped conceptualize and analyze computational experiments and co-wrote the paper. D.R.K. and F.D.M. conceptualized and designed experiments and co-wrote the paper.

ACKNOWLEDGMENTS

This work was funded by CIHR grants MOP-125945 and 142267 and the Canadian Stem Cell Network. F.D.M. is an HHMI Senior International Research Scholar, and F.D.M. and D.R.K. are Canada Research Chairs. S.A.Y. was funded by an OIRM Fellowship and G.Y. by a Brain Canada Fellowship. We thank Sarah Burns, Wenliau Qiao, Nish Patel, and Ran Kafri for discussions and assistance/advice and Jonathan Krieger/Paul Taylor at the HSC SPARC BioCentre as well as TCAG.

Received: February 29, 2016
Revised: June 29, 2016
Accepted: July 21, 2016
Published: August 18, 2016

REFERENCES

Elsen, G.E., Hodge, R.D., Bedogni, F., Daza, R.A., Nelson, B.R., Shiba, N., Reiner, S.L., and Hevner, R.F. (2013). The protomap is propagated to cortical plate neurons through an Eomes-dependent intermediate map. Proc. Natl. Acad. Sci. USA *110*, 4081–4086.

Gallagher, D., Norman, A.A., Woodard, C.L., Yang, G., Gauthier-Fisher, A., Fujitani, M., Vessey, J.P., Cancino, G.I., Sachewsky, N., Woltjen, K., et al. (2013). Transient maternal IL-6 mediates long-lasting changes in neural stem cell pools by deregulating an endogenous self-renewal pathway. Cell Stem Cell *13*, 564–576.

Gauthier-Fisher, A., and Miller, F.D. (2013). Environmental cues and signalling pathways that regulate neural precursor development. In Patterning and Cell Type Specification in the Developing CNS and PNS: Comprehensive Developmental Neuroscience, J.L. Rubenstein and P. Rakic, eds. (Elsevier Press), pp. 355–383.

Gauthier-Fisher, A., Lin, D.C., Greeve, M., Kaplan, D.R., Rottapel, R., and Miller, F.D. (2009). Lfc and Tctex-1 regulate the genesis of neurons from cortical precursor cells. Nat. Neurosci. *12*, 735–744.

Haydar, T.F., Wang, F., Schwartz, M.L., and Rakic, P. (2000). Differential modulation of proliferation in the neocortical ventricular and subventricular zones. J. Neurosci. *20*, 5764–5774.

Igarashi, K., Garotta, G., Ozmen, L., Ziemiecki, A., Wilks, A.F., Harpur, A.G., Larner, A.C., and Finbloom, D.S. (1994). Interferon-gamma induces tyrosine phosphorylation of interferon-gamma receptor and regulated association of protein tyrosine kinases, Jak1 and Jak2, with its receptor. J. Biol. Chem. *269*, 14333–14336.

Jing, S., Yu, Y., Fang, M., Hu, Z., Holst, P.L., Boone, T., Delaney, J., Schultz, H., Zhou, R., and Fox, G.M. (1997). GFRalpha-2 and GFRalpha-3 are two new receptors for ligands of the GDNF family. J. Biol. Chem. *272*, 33111–33117.

Kirouac, D.C., Ito, C., Csaszar, E., Roch, A., Yu, M., Sykes, E.A., Bader, G.D., and Zandstra, P.W. (2010). Dynamic interaction networks in a hierarchically organized tissue. Mol. Syst. Biol. *6*, 417.

Kusek, G., Campbell, M., Doyle, F., Tenenbaum, S.A., Kiebler, M., and Temple, S. (2012). Asymmetric segregation of the double-stranded RNA binding protein Staufen2 during mammalian neural stem cell divisions promotes lineage progression. Cell Stem Cell *11*, 505–516.

Lundberg, E., Fagerberg, L., Klevebring, D., Matic, I., Geiger, T., Cox, J., Algenäs, C., Lundeberg, J., Mann, M., and Uhlen, M. (2010). Defining the transcriptome and proteome in three functionally different human cell lines. Mol. Syst. Biol. *6*, 450.

Lundgren, T.K., Nakahata, K., Fritz, N., Rebellato, P., Zhang, S., and Uhlén, P. (2012). RET PLCγ phosphotyrosine binding domain regulates Ca2+ signaling and neocortical neuronal migration. PLoS ONE *7*, e31258.

McDonald, C.A., Yang, J.Y., Marathe, V., Yen, T.Y., and Macher, B.A. (2009). Combining results from lectin affinity chromatography and glycocapture approaches substantially improves the coverage of the glycoproteome. Mol. Cell. Proteomics *8*, 287–301.

Ménard, C., Hein, P., Paquin, A., Savelson, A., Yang, X.M., Lederfein, D., Barnabé-Heider, F., Mir, A.A., Sterneck, E., Peterson, A.C., et al. (2002). An essential role for a MEK-C/EBP pathway during growth factor-regulated cortical neurogenesis. Neuron *36*, 597–610.

Noctor, S.C., Flint, A.C., Weissman, T.A., Dammerman, R.S., and Kriegstein, A.R. (2001). Neurons derived from radial glial cells establish radial units in neocortex. Nature *409*, 714–720.

Nomaru, H., Sakumi, K., Katogi, A., Ohnishi, Y.N., Kajitani, K., Tsuchimoto, D., Nestler, E.J., and Nakabeppu, Y. (2014). Fosb gene products contribute to excitotoxic microglial activation by regulating the expression of complement C5a receptors in microglia. Glia *62*, 1284–1298.

Parikshak, N.N., Luo, R., Zhang, A., Won, H., Lowe, J.K., Chandran, V., Horvath, S., and Geschwind, D.H. (2013). Integrative functional genomic analyses implicate specific molecular pathways and circuits in autism. Cell *155*, 1008–1021.

Parikshak, N.N., Gandal, M.J., and Geschwind, D.H. (2015). Systems biology and gene networks in neurodevelopmental and neurodegenerative disorders. Nat. Rev. Genet. *16*, 441–458.

Pozas, E., and Ibáñez, C.F. (2005). GDNF and GFRalpha1 promote differentiation and tangential migration of cortical GABAergic neurons. Neuron *45*, 701–713.

Qiao, W., Quon, G., Csaszar, E., Yu, M., Morris, Q., and Zandstra, P.W. (2012). PERT: a method for expression deconvolution of human blood samples from varied microenvironmental and developmental conditions. PLoS Comput. Biol. *8*, e1002838.

Qiao, W., Wang, W., Laurenti, E., Turinsky, A.L., Wodak, S.J., Bader, G.D., Dick, J.E., and Zandstra, P.W. (2014). Intercellular network structure and regulatory motifs in the human hematopoietic system. Mol. Syst. Biol. *10*, 741.

Raballo, R., Rhee, J., Lyn-Cook, R., Leckman, J.F., Schwartz, M.L., and Vaccarino, F.M. (2000). Basic fibroblast growth factor (Fgf2) is necessary for cell proliferation and neurogenesis in the developing cerebral cortex. J. Neurosci. *20*, 5012–5023.

Roy, S.K., Hu, J., Meng, Q., Xia, Y., Shapiro, P.S., Reddy, S.P., Platanias, L.C., Lindner, D.J., Johnson, P.F., Pritchard, C., et al. (2002). MEKK1 plays a critical role in activating the transcription factor C/EBP-beta-dependent gene expression in response to IFN-gamma. Proc. Natl. Acad. Sci. USA *99*, 7945–7950.

Schiess, R., Mueller, L.N., Schmidt, A., Mueller, M., Wollscheid, B., and Aebersold, R. (2009). Analysis of cell surface proteome changes via label-free, quantitative mass spectrometry. Mol. Cell. Proteomics *8*, 624–638.

Villeda, S.A., Luo, J., Mosher, K.I., Zou, B., Britschgi, M., Bieri, G., Stan, T.M., Fainberg, N., Ding, Z., Eggel, A., et al. (2011). The ageing systemic milieu negatively regulates neurogenesis and cognitive function. Nature *477*, 90–94.

Worby, C.A., Vega, Q.C., Zhao, Y., Chao, H.H., Seasholtz, A.F., and Dixon, J.E. (1996). Glial cell line-derived neurotrophic factor signals through the RET receptor and activates mitogen-activated protein kinase. J. Biol. Chem. *271*, 23619–23622.

Zeisel, A., Muñoz-Manchado, A.B., Codeluppi, S., Lönnerberg, P., La Manno, G., Juréus, A., Marques, S., Munguba, H., He, L., Betsholtz, C., et al. (2015). Brain structure. Cell types in the mouse cortex and hippocampus revealed by single-cell RNA-seq. Science *347*, 1138–1142.